Optimal Estimation of Conjugate Shifts in Position and Momentum by Classically Correlated Probes and Measurements

Kimin Park,[1] Changhun Oh,[2,3] Radim Filip,[1] and Petr Marek[1,*]

[1] *Department of Optics, Palacký University, 17. listopadu 1192/12, Olomouc 771 46, Czech Republic*
[2] *Department of Physics and Astronomy, Seoul National University, Seoul 08826, Korea*
[3] *Pritzker School of Molecular Engineering, The University of Chicago, Chicago, Illinois 60637, USA*

(Received 18 October 2021; revised 9 May 2022; accepted 2 June 2022; published 25 July 2022)

Multiparameter estimation is necessary for force sensing due to simultaneous and nontrivial small changes of position and momentum. The design of quantum probes that allow simultaneous estimation of all parameters is therefore an important task. The optimal methods for estimation of the conjugate changes of position and momentum of quantum harmonic oscillator employ probes in entangled or quantum non-Gaussian states. We show that the same results can be obtained in a significantly more feasible fashion by employing independent sets of differently squeezed Gaussian states classically correlated with position or momentum measurements. This result demonstrates an unexplored power of a classical correlation between the probe states and measurements directly applicable to force sensing.

DOI: 10.1103/PhysRevApplied.18.014060

I. INTRODUCTION

The main goal of quantum metrology lies in finding and achieving the ultimate limits on measuring parameters of known physical processes [1–4]. It can be applied to estimation of single [1,2,5–8] as well as multiple parameters [9–18]. The key principle lies in paying attention to the quantum state of the employed probes such as modes of light [19,20], mechanical modes of trapped ions [21–23], collective modes of spins in a magnetic field [24–26], mechanical modes of optomechanical oscillators [27–29], or in principle any other quantum system.

Quantum multiparameter estimation aims to discern a set of real parameters $\theta = (\theta_1, \ldots, \theta_M)$ that characterize a given channel. This is realized by preparing an ensemble of probes in a known quantum state, sending them through the channel, subjecting them to quantum measurement, and subsequently applying an estimation strategy to produce a set of unbiased estimators $\tilde{\theta} = (\tilde{\theta}_1, \ldots, \tilde{\theta}_M)$. The quality of the estimation depends on the difference between the estimators and the true values and it can be conservatively evaluated by the mean quadratic variances $v_j := \langle(\theta_j - \tilde{\theta}_j)^2\rangle$ [3]. For any particular measurement strategy, these variances are bounded by the inverse of the classical Fisher information (CFI). Their ultimate limit is given by the Holevo-Cramer-Rao (HCR) bound [3,12] that can be obtained by minimization over all possible measurement strategies, which can, in many cases, be only done numerically. Numerical computation can be also used to obtain the Nagaoka-Hayashi bound for separable single-copy measurements [30,31]. The variances are also lower bounded by the inverse of the quantum Fisher information (QFI) obtained either from symmetric or right-logarithmic derivatives [3,6,13] but this bound is not always tight for multiparameter quantum estimation. The optimal probe state is one that offers the maximal precision for constraints limiting probe preparation, sampling, and measurement. Some commonly employed constraints are preparing the probe states as identical copies of a specific quantum state [1,12,32] and maximal energy of the probes [23,33–35].

One essential task of quantum sensing is estimation of parameters of a small mechanical, electrical, magnetic, or optical force [36–38]. A particular scenario commonly studied in this context is the simultaneous estimation of the position and momentum—two parameters of quantum displacement acting on a state of a harmonic oscillator [33–35,39]. Beyond the considerable fundamental interest [12,18], this basic measurement is already relevant for the calibration of continuous-variable quantum key distribution in optical systems [40], the estimation of weak electric fields with trapped ion crystals [41], or the estimation of temperature in ultracold lattice gases [42]. On the elementary level, the displacement is represented by the unitary evolution operator $D(\mu + i\nu) = e^{-i\nu X - i\mu P}$, where

*marek@optics.upol.cz

X and P are the quadrature operators of the optical field with commutator $[X,P] = i$ and μ and ν are the unknown parameters. This scenario is an example of a Gaussian shift model [12] and the difficulty lies in simultaneously estimating values of the noncommuting operators X and P bound together by Heisenberg uncertainty relations.

Two approaches have been suggested to overcome this issue. The first utilizes a set of identical probes in two-mode squeezed quantum entangled states, in which both quadratures can be simultaneously estimated with high precision due to the dense coding effect [33]. The second employs a set of identical single-mode probes prepared in quantum states that are superpositions of differently displaced squeezed states [34,39]. In this case, the possibility of simultaneous estimation is the consequence of the rich sub-Planck structure of the nonclassical and highly non-Gaussian quantum states. A similar technique has also been suggested for estimation of the amplitude of the displacement operation, which is only a single parameter but depends on the two noncommuting quantities X and P. The amplitude is efficiently estimated by employing probes in Fock states of the harmonic oscillator [23,43], which are again non-Gaussian states with a rich sub-Planck structure. These approaches are argued to be optimal in the sense that the proposed measurement strategies saturate the HCR bound of the probe states and the probe states have the minimal energy that allows this HCR [23,33–35].

In this paper, we show that the optimal estimation of the two parameters of displacement can, on average and in the limit of large number of probes, also be achieved by measuring the two parameters independently by using two sets of factorized quantum states, squeezed in position or momentum, and measurement of the respective variable. This approach, inspired by some techniques of quantum process tomography [44–46], leads to the same mean quadratic error as the methods based on entangled two-mode squeezed states [33] or quantum non-Gaussian states [34,39] with the same energy of the individual probes. This performance is obtained even though the sequence of squeezed states is generally more feasible to implement.

II. METHODS

The standard estimation scheme with a single set of identical probes represented by quantum state $\rho^{\otimes N}$ and a single measurement strategy given by positive-operator-valued measure (POVM) Π is illustrated in Fig. 1(a). Each probe independently interacts with the channel and is subsequently measured. Note that each individual probe can be in an entangled state of several subsystems, only some of which interact with the channel. The protocol that we propose is illustrated in Fig. 1(b) and it employs several sets of different probes, each one prepared in one of the different states ρ_n. Their collective state can therefore be represented by $\bigotimes_n \rho_n^{\otimes N_n}$, where the numbers of probes

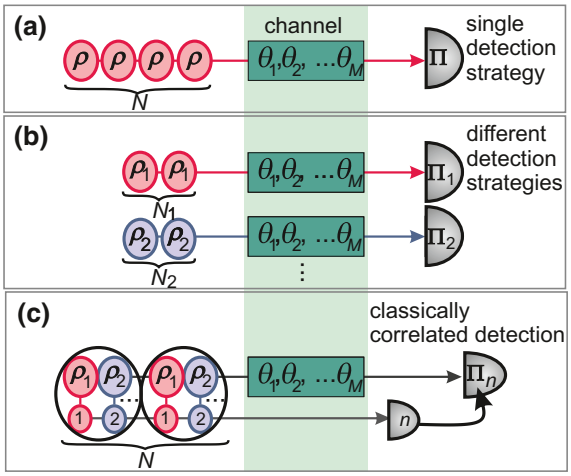

FIG. 1. (a) The standard scenario of quantum parameter estimation with a set of N identical probes ρ that interact with the channel, undergo transformation given by parameters $\theta_1, \ldots, \theta_M$, and are measured by measurements given by POVM Π. (b) Quantum parameter estimation by N different separate probes $\rho_1, \rho_2, \ldots$ that individually interact with the channel and are individually measured by fixed measurements with POVMs $\Pi_1, \Pi_2, \ldots$ classically correlated with the respective probes. (c) Quantum parameter estimation by N different separate probes, such as those in Fig. 1(b), effectively represented by estimation with a set of identical classically correlated states given in Eq. (1) of probes $\rho_1, \rho_2 \cdots$ and their respective orthonormal markers, denoted by $n = 1, 2, \ldots$. The classically correlated measurement in Eq. (2) consists of detection of the marker state $|n\rangle$ followed by feed-forward setting of the particular detector to the one with POVM Π_n.

satisfy $\sum_n N_n = N$. Each probe interacts with the channel that transforms its state into $\rho_n(\theta)$ and is measured by a measurement Π_n tailored to the respective set. Each such measurement is represented by POVM elements $\{\Pi_n(o_n)\}$ with the corresponding measurement results $\{o_n\}$. We do not assume specific dimensionality of the measurement: the measurement results o_n are vectors of real values. The estimators $\tilde{\theta}$ can now be obtained from the classical probability distributions $P(o_n)$.

For the sake of straightforward comparison, we can also express the protocol with sets of different probes in an effective form that utilizes a single set of identical classically correlated probes [see Fig. 1(c)]. Note that this is only for the sake of comparison and clarity: in practical application, it is not necessary. In this approach, each individual probe state can be expressed as a single classically correlated quantum state

$$\rho_T = \sum_n w_n |n\rangle\langle n| \otimes \rho_n, \tag{1}$$

where $w_n = N_n/N$ are the relative probe weights and $|n\rangle$ are arbitrary orthonormal states. Their role is to serve as classical markers for the detectors, differentiating the

individual probe states in the mixture. The probe is then subjected to a trace-preserving quantum channel that transforms the state into $\rho_T' = \sum_{n=0} w_n |n\rangle\langle n| \otimes \rho_n'(\theta)$, leaving the marker states $|n\rangle$ as well as the weights w_n unchanged.

The probe state ρ_T' now needs to be measured to extract the information imparted by the channel. In this effective model, we consider this measurement to be composed of two parts. First, we measure the marker states. Since they are orthogonal and not affected by the channel, the measurement always returns the correct marker, which is used to set the desired measurement for the probe. Formally, the global POVM of the measurement is such that the measured values are vectors of real values $[n, o_n]$, each of which corresponds to the POVM element

$$|n\rangle\langle n| \otimes \Pi_n(o_n). \tag{2}$$

The joint probability distribution obtained by this measurement is then represented by the probability distribution

$$f(n, o_n) = \mathrm{Tr}[\rho_T' |n\rangle\langle n| \otimes \Pi_n(o_n)] \tag{3}$$

and is essentially a finite sequence of probability distributions $f(o_n)$ for each individual combination of the probe state and its respective measurement. The joint probability distribution can be used to evaluate elements of the CFI matrix $\mathbf{C}_T$ for any pair of channel parameters θ_j, θ_l:

$$\mathbf{C}_T(j,l) = \sum_{n=1} \int do_n \frac{(\partial_{\theta_j} f(n, o_n) \partial_{\theta_l} f(n, o_n))}{f(n, o_n)}, \tag{4}$$

where the integration is always over the full support of variable vector o_n and the sum is over all the marker states in Eq. (1). Since $f(n, o_n) = w_n f_n(o_n)$, where $f_n(o_n) = \mathrm{Tr}[\rho_n \Pi(o_n)]$ is the probability distribution for the specific combination of probe and measurement, we can see that the CFI matrix obtained in this way is equal to the weighted sum of CFI matrices of the individual probe-measurement pairs with weights w_n, $\mathbf{C}_T = \sum_n w_n \mathbf{C}_n$. It is not as straightforward to obtain the tight HCR bound and this usually needs to be performed numerically [47]. On the other hand, the nontight Cramer-Rao bound based on the QFI matrix can easily be obtained from $\mathbf{Q}_T = \sum_n w_n \mathbf{Q}_n$, which follows from the additivity property. Note that in the following, we are interested in the comparison of a specific estimation scenario, for which the CFI will be sufficient.

III. RESULTS

Let us now turn to the specific case of estimating the two parameters of the displacement operation $D(\mu + i\nu) = e^{-i\nu X - i\mu P}$. The entanglement-based protocol [33,35,39] for simultaneous estimation of μ and ν is illustrated in Fig. 2(a). Each probe is an entangled two-mode squeezed state that can be prepared by interference of two orthogonally squeezed states on a balanced beam splitter. The state of the probe can be explicitly written in the X representation as

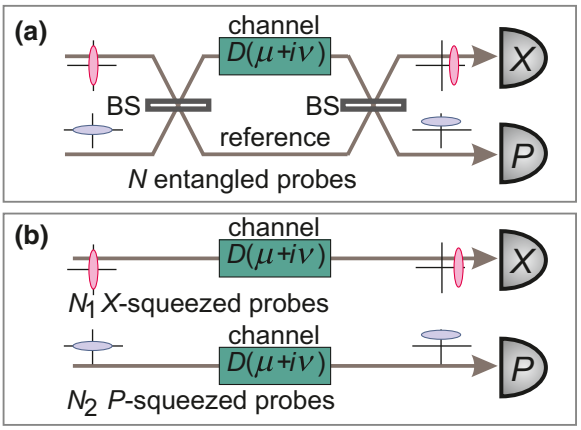

FIG. 2. The estimation of two parameters of the displacement operation $D(\mu + i\nu) = e^{-i\nu X - i\mu P}$. (a) An entanglement-based scenario in which each of the N probes is prepared in an entangled state by interfering two orthogonally squeezed states on a balanced beam splitter (BS). One of the modes passes through the estimated channel, while the second serves as a reference. The modes are recombined on another balanced beam splitter and quadratures X and P are measured by homodyne detectors. (b) Estimation by two sets of different probes of which N_1 is squeezed in X and N_2 is squeezed in P, $N_1 + N_2 = N$. Each probe passes through the channel and the corresponding quadratures are measured by homodyne detection.

$$|\psi\rangle = \frac{1}{2\pi} \int dx\, dy\, e^{-(x+y)^2/4e^{-2r}} e^{-(x-y)^2/4e^{2r}} |x, y\rangle. \tag{5}$$

This is an entangled quantum state defined by the nonclassical correlations $\langle (X_1 - X_2)^2 \rangle = \langle (P_1 + P_2)^2 \rangle = e^{-2r}$ of the quadrature operators of the respective two modes. The optimal measurement is composed of another balanced beam splitter followed by homodyne detectors measuring quadratures X and P of the two output ports, [35], which produce the joint probability distribution

$$f(x,p) = \frac{1}{\pi e^{-2r}} \exp\left[-\frac{(x - \mu/\sqrt{2})^2}{e^{-2r}} - \frac{(p - \nu/\sqrt{2})^2}{e^{-2r}} \right]. \tag{6}$$

From here, we can arrive at a diagonal CFI matrix with elements $C_E(1,1) = C_E(2,2) = e^{2r}$ that saturate the HCR bound [33] for the case when the two displacements are given equal importance. When this is not the case, the protocol can be adjusted by changing the symmetry of the probe as well as that of the final measurement. The HCR can be reached in all cases [39].

The particular application of method depicted in Fig. 1(b) is illustrated in Fig. 2(b). It is based on two sets of vacuum states squeezed either in the X or the P quadrature, which are measured by homodyne detection of the

respective squeezed quadrature. We can formally write the effective mixed state given in Eq. (1) as

$$\rho_T = w_1|\phi\rangle\langle\phi| \otimes S|0\rangle\langle 0|S^\dagger + w_2|\phi^\perp\rangle\langle\phi^\perp| \otimes S^\dagger|0\rangle\langle 0|S, \tag{7}$$

where $|\phi\rangle$ and $|\phi^\perp\rangle$ are the orthonormal marker states, $|0\rangle$ is the vacuum state of quantum harmonic oscillator, and S is a squeezing operator such that $S|0\rangle$ is a squeezed vacuum state with variance $\mathrm{var}X = (1/2)e^{-2r}$. Note that the squeezing is chosen in such a way that the probe states are the same as those used to compose the entangled state given in Eq. (5) in the entanglement-based protocol. As a consequence, the same energy passes through the channel during each run of the protocol and they are therefore directly comparable. The homodyne measurements aligned with the squeezed quadrature of the probe states are represented by POVM elements

$$\begin{aligned}\Pi(1,q) &= |\phi\rangle\langle\phi| \otimes |X = q\rangle\langle X = q|,\\ \Pi(2,q) &= |\phi^\perp\rangle\langle\phi^\perp| \otimes |P = q\rangle\langle P = q|,\end{aligned} \tag{8}$$

where $|X = q\rangle$ and $|P = q\rangle$ represent the X and P quadrature eigenstates with eigenvalue q, respectively. These measurements produce a pair of probability distributions $f_X(x) = w_1 \exp(-(x-\mu)^2/e^{-2r})/\sqrt{\pi e^{-2r}}$ and $f_P(p) = w_2 \exp(-(x-\mu)^2/e^{-2r})/\sqrt{\pi e^{-2r}}$ that can now be used to obtain the CFI matrix, which is diagonal, with matrix elements $C_S(1,1) = 2w_1e^{-2r}$ and $C_S(2,2) = 2w_2e^{-2r}$. For equal importance of the two estimated parameters, the weights can be set to $w_1 = w_2 = 0.5$ and the matrix is identical to the one from the entanglement-based protocol. This can also be seen from the equality $f(x,p) = 2f_X(x\sqrt{2})f_P(p\sqrt{2})$. The differing importance of the parameters can be then taken into account by adjusting the weights w_1 and w_2. In all cases, the achieved variances are identical to those obtained in Ref. [39] and therefore also saturate the HCR bounds of the entanglement-based protocol. Since the energies of the probes that pass through the channel are also identical, the protocol based on separate probes can be also considered optimal.

At the level of physical intuition, the equivalence between the schemes can be understood as follows. In the entanglement-based scheme, the displacement is encoded simultaneously into both quadratures and entanglement is used, via the dense-coding effect [48], to measure them simultaneously. In each run of the experiment, both variables are measured but there is a cost. The interference on the beam splitter attenuates the displacement so that each homodyne detector effectively detects only half of it. On the other hand, for two sets of squeezed probes, each individual run detects displacement only in a single quadrature. However, it can detect it fully, with no loss of information. Furthermore, from a practical perspective, the interference in state preparation and detection required by the entanglement-based protocol adds to the difficulty of the implementation and causes mode-matching losses. For a more thorough analysis on how the losses affect the performance of the protocols, see the Appendix A.

A related problem is the estimation of the amplitude of the displacement $|\alpha| = \sqrt{\mu^2 + \nu^2}$ [23,43]. This is essentially an estimation of a single parameter that is related to the two parameters of the displacement. It has been shown, in Ref. [23], that the optimal estimation strategy with regard to the energy of the probe consists of utilizing photon-number Fock states and photon-number measurements. For this protocol, the CFI $\mathbf{C}_n = 4\langle a^\dagger a\rangle + 2$ saturates the QFI. Remarkably, even in this case we can approach this performance with the protocol based on the two sets of separately squeezed probes given in Eq. (7), with balanced weights $w_1 = w_2 = 0.5$ measured by homodyne detection. The CFI matrix for simultaneous estimation of amplitude $|\alpha|$ and phase ϕ can be found to be

$$\mathbf{C} = 2(\langle a^\dagger a\rangle + 1 + \sqrt{\langle a^\dagger a\rangle^2 + \langle a^\dagger a\rangle}) \begin{pmatrix} 1 & 0 \\ 0 & |\alpha|^2 \end{pmatrix}, \tag{9}$$

where we use $\langle a^\dagger a\rangle = (e^{2r} + e^{-2r} - 2)/4$ to allow effective comparison with Fock states and their energy. We can see that in the limit of large energy, the CFI-matrix element $\mathbf{C}(1,1)$, corresponding to estimation of $|\alpha|$, approaches the QFI, and thus the ultimate precision, of the single-parameter estimation of the Fock-based scenario. For example, with average energy $\langle a^\dagger a\rangle = 5$, the CFI for the Fock-state approach is $\mathbf{C}_n = 22$, while for the respective squeezed states with 13 dB squeezing, it is $\mathbf{C}_S = 21.95$. At the same time, the approach with independent squeezed states also provides information about the phase of the displacement that is completely disregarded by the Fock-state approach. The squeezed states are more vulnerable to the adverse effects of loss, because the environment-mode vacuum fluctuations always lower bound the achievable variance (see the Appendix). However, their experimental preparation, especially in the optical setting [49–53], is—compared to photon-number states and photon-number-resolving detectors [54–57]—significantly more feasible.

IV. CONCLUSIONS

We shown that the two parameters of coherent displacement can be independently estimated by two sets of probes prepared in squeezed states and classically correlated position and momentum measurements. The achievable errors are the same as for the optimal methods taking advantage of quantum entanglement of two-mode squeezed states [33,35,39] or the sub-Planck structure of quantum non-Gaussian probe states [34]. The equivalence holds

asymptotically in the limit of large number of probes, which is a common assumption in quantum estimation scenarios. This finding has several interesting ramifications.

It presents a more feasible scheme for the practical estimation of quantum displacement [40–42], because the use of sets of differently squeezed states is more feasible and therefore cheaper [58] than the entangled [33,35,39] or quantum non-Gaussian states [34]. We expect it can have a direct impact on sensing of mechanical, electric, magnetic, and optical forces [36–38]. It also demonstrates that even in multiparameter quantum estimation, it is not necessary to simultaneously estimate all the parameters in each trial and that mixed states, together with classically correlated measurements, can be optimal. And, finally, it also means that the estimation of the two displacement parameters, which is an often-studied scenario in quantum metrology, is not a challenging multiparameter estimation problem, because the two parameters can be efficiently estimated independently. The realization of this and the ability to recognize such scenarios will improve our general understanding of quantum multiparameter estimation protocols and stimulate further theoretical and experimental research. In the future, we hope to analyze the general model arbitrary observables and conclusively identify the scenarios, in which the use of separable probes is advantageous.

ACKNOWLEDGMENTS

P.M. acknowledges Project 22-08772S of the Grant Agency of the Czech Republic (GACR). K.P. acknowledges the Ministry of Education, Youth and Sports (MEYS) of the Czech Republic (Grant Agreement No. 8C20002) and the funding from the European Union Horizon 2020 (2014-2020) research and innovation framework program under Grant Agreement No. 731473 ["Short-range optical Quantum Connections" (ShoQC)]. Project ShoQC has received funding from the QuantERA ERA-NET Cofund in Quantum Technologies implemented within the European Union Horizon 2020 program. R.F. acknowledges the Ministry of Education, Youth and Sports under Grant Agreements No. CZ.02.1.01/0.0/0.0/16_026/0008460 and No. LTAUSA19099. C.O. acknowledges support from the National Science Foundation (NSF) (OMA-1936118). K.P., P.M., and R.F. have further been supported by the European Union 2020 research and innovation program (CSA—Coordination and support action, H2020-WIDESPREAD-2020-5) under Grant Agreement No. 951737 (NONGAUSS).

APPENDIX A: PRACTICAL COMPARISON WITH LOSSES

Let us now expand the model with separate probes to incorporate realistic losses. Since losses are a practical consideration, we consider only the CFI that sets the limit of practical measurement tools. Losses in the state preparation manifest by changing the variance matrix of the input state. The variances of the two quadrature operators for a squeezed state need to be represented by two independent values: V_S for the squeezed quadrature and V_A for the antisqueezed one. In turn, losses in the channel can be modeled as virtual beam splitters that couple the respective mode to a bath in vacuum state. The losses can appear either before or after the estimated operation. These scenarios only differ by a constant scaling factor arising from loss of the displacement. For the sake of comparison between the protocols, we can therefore consider losses taking place only before the estimated operation.

For the swapping protocol, the model is simple. The initial states are squeezed, with variance V_S, and pass through the lossy channel with intensity transmission coefficient η_1. Since the measurement always resolves the squeezed quadrature, the measurement statistics will again be a Gaussian function, now with variances

$$V_{\text{out}} = \eta_1 V_S + (1-\eta_1)\frac{1}{2}. \tag{A1}$$

This leads to a diagonal CFI matrix for the whole measurement that has elements $C_S(1,1) = C_S(2,2) = 2/V_{\text{out}}$. We can see that losses in the channel are no fundamentally different from losses in the preparation. In the end, the only thing that matters is the available squeezing.

The description is more involved in the case of the entanglement-based protocol. Here, it is best to start from the variance matrix of the initial pair of states, $\Sigma = \text{diag}(V_S, V_A, V_A, V_S)$, and use it to find variance matrix of the two modes right before the measurement by subjecting it to the sequence of operations

$$\Sigma_{\text{out}} = O_{\text{BS}}^T Y O_{\text{BS}} \Sigma_{\text{in}} O_{\text{BS}}^T Y O_{\text{BS}} + \frac{I}{2} - \frac{1}{2} O_{\text{BS}}^T Y^2 O_{\text{BS}}, \tag{A2}$$

where O_{BS} is the orthogonal matrix describing the action of the balanced beam splitter, I is a 4×4 unit matrix, and $Y = \text{diag}(\sqrt{\eta_1}, \sqrt{\eta_1}, \sqrt{\eta_2}, \sqrt{\eta_2})$ represents the action of the two lossy channels. The two homodyne detectors, which measure quadratures x_1 and p_2, then return data with a Gaussian distribution, with mean values given by the displacement and variance matrix $\Sigma_m = \text{diag}(V_m, V_m)$. This matrix is obtained by removing second and third rows and columns from Eq. (A2) and the variances are

$$V_m = \frac{1}{4}[(V_S + V_A - 1)(\eta_1 + \eta_2) + 2\sqrt{\eta_1\eta_2}(V_S - V_A) + 2]. \tag{A3}$$

Since the matrix is diagonal with identical diagonal elements, the elements of the diagonal CFI matrix can be obtained as $C_E(1,1) = C_E(2,2) = 2/V_m$ and the comparison between the swapping and the entanglement-based

protocols fully depends on the two variances given in Eqs. (A1) and (A3).

The first observation that we can make is that when $\eta_1 = \eta_2$, the two protocols are again identical. This is no longer the case when the equality does not hold. From the form of Eq. (A3), we can see that it describes a parabola for variable $y_2 = \sqrt{\eta_2}$. This parabola has a minimum for

$$\sqrt{\eta_2} = \sqrt{\eta_1}\frac{V_A - V_S}{V_A + V_S - 1} > \sqrt{\eta_1}, \tag{A4}$$

which means that for any loss η_1 in channel 1 containing the displacement operation to be estimated, there is a range of values $\eta_2 < \eta_1$ for loss in channel 2 for which the protocol has an advantage over the swapping scheme, which only uses channel 1. The exact range of values of η_2 depends on the properties of the state. In the limit of large squeezing, in which V_A necessarily approaches infinity, it is optimal to have $\eta_2 = \eta_1$. Interestingly, for the fixed measurement this could lead to the counterintuitive scenario in which it would be beneficial to add artificial losses to the reference arm to achieve an optimal regime.

To better understand this behavior, we can consider an entanglement-based protocol that is optimized for the channel transmission coefficient η_1 and η_2. The initial quantum states are the same two orthogonally squeezed vacuum states with variances V_A and V_S but the interferometer is now composed of two beam splitters with general coefficients t_1, r_1 and t_2, r_2. In such a scenario, the diagonal CFI-matrix elements can be found to be $C_E(1,1) = t_2^2/V_1, \quad C_E(2,2) = r_2^2/V_2$, with

$$\begin{aligned} V_1 &= 2t_1r_1t_2r_2\sqrt{\eta_1\eta_2}(V_A - V_S) \\ &\quad + \frac{1 - t_2^2\eta_1 - r_2^2\eta_2}{2} + \eta_2 r_2^2(t_1^2V_A + r_1^2V_S) \\ &\quad + \eta_1 t_2^2(r_1^2V_A + t_1^2V_S), \\ V_2 &= 2t_1r_1t_2r_2\sqrt{\eta_1\eta_2}(V_A - V_S) \\ &\quad + \frac{1 - t_2^2\eta_2 - r_2^2\eta_1}{2} + \eta_1 r_2^2(t_1^2V_A + r_1^2V_S) \\ &\quad + \eta_2 t_2^2(r_1^2V_A + t_1^2V_S). \end{aligned} \tag{A5}$$

We can see that the two diagonal elements are not necessarily equal. This is a consequence of the asymmetrical setup and it separates the approach from the swapping scheme, which is always symmetrical with respect to the two observable quantities. To jointly describe estimation of both quantities, we consider the determinant of the CFI matrix and numerically maximize it with respect to the interferometer parameters t_1, r_1, t_2, and r_2. We can then compare the optimal CFI to that of the swapping protocol by means of a ratio $|C_E|/|C_F|$, which is larger than 1 when the entanglement protocol has the advantage and smaller than 1 otherwise. An example of the behavior is shown in Fig. 3.

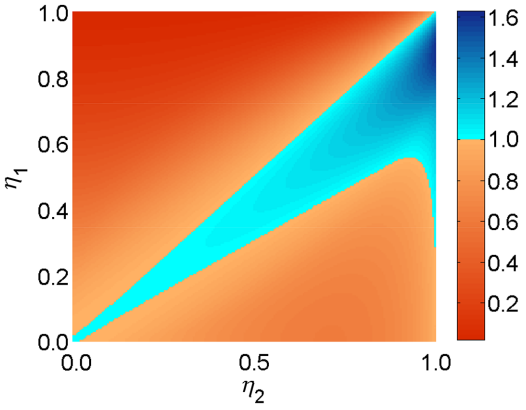

FIG. 3. A comparison of the CFI-matrix determinant ratio $\frac{|C_E|}{|C_F|}$ relative to the transmission coefficients η_1 and η_2 of the two channels. The initial squeezed quantum states are described by $V_S = e^{-2}/2$ and $V_A = e^2/2$. The parameters of the entanglement-based scheme are optimized. In the blue area, the entanglement-based protocol has the advantage; in the red area, swapping of different probes has the advantage.

We can see that the swapping protocol has always the advantage when $\eta_1 > \eta_2$. However, when $\eta_2 > \eta_1$, the entanglement-based protocol has an advantage only for some values of η_2 and those values are close to η_1—similar to the case without the optimization, there are situations in which it is actually disadvantageous to have losses that are too low. The reason for this is not completely clear but it can follow from the reduced symmetry of the scenario. Nevertheless, with optimization of loss and the interferometer parameters, the entanglement-based protocol can always be made to have an advantage For $\eta_2 > \eta_1$.

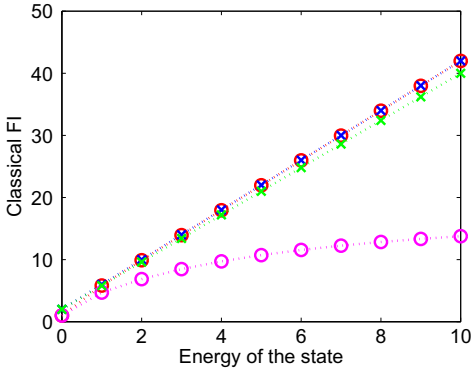

FIG. 4. The comparison of the CFI for estimation of the amplitude of displacement with lossy states: blue crosses, Fock-state approach with $\eta = 1$; green crosses, Fock-state approach with $\eta = 0.95$; red circles, squeezed-state approach with $\eta = 1$; magenta circles, squeezed-state approach with $\eta = 0.95$.

This advantage, however, vanishes in the limit of large squeezing.

In estimation of the amplitude of the displacement without regard to the phase, we can again use Eq. (A1) and, under the assumption that the states are pure with variance $V_S = e^{-2r}/2$ before the channel, find the relevant classical Fisher-information-matrix element equal to

$$C_S(1,1) = \frac{1}{2V_{\text{out}}}, \tag{A6}$$

where the initial energy of the state is given by $\langle a^\dagger a\rangle = (e^{2r} + e^{-2r} - 2)/4$. For the scheme employing the Fock states, we can evaluate the quantum Fisher information because it is saturated by the CFI. The quantum FI for Fock state $|n\rangle$ can now be found to be

$$Q_F = 2\sum_{k=0}^{n} \binom{n}{k} \eta^k (1-\eta)^{n-k}(2k+1). \tag{A7}$$

The comparison of the CFI for the two scenarios and for $\eta = 1$ and $\eta = 0.95$ is shown in Fig. 4. We can see that in the ideal scenario with $\eta = 1$, the two approaches are practically identical. However, while the losses only marginally affect the Fock-state scenario, they significantly reduce the performance of the squeezed-state protocol. This is the consequence of the form of Eq. (A1), which is lower bounded by the losses regardless of the initial energy of the state.

[1] V. Giovannetti, S. Lloyd, and L. Maccone, Advances in quantum metrology, Nat. Photonics **5**, 222 (2011).

[2] R. Demkowicz-Dobrzański, M. Jarzyna, and J. Kołodyński, in *Progress in Optics* (Elsevier, North Holland, 2015), p. 345.

[3] A. Holevo, *Probabilistic and Statistical Aspects of Quantum Theory* (Scuola Normale Superiore, Pisa, 2011).

[4] E. Polino, M. Valeri, N. Spagnolo, and F. Sciarrino, Photonic quantum metrology, AVS Quantum Sci. **2**, 024703 (2020).

[5] L. Pezzè, A. Smerzi, M. K. Oberthaler, R. Schmied, and P. Treutlein, Quantum metrology with nonclassical states of atomic ensembles, Rev. Mod. Phys. **90**, 035005 (2018).

[6] M. G. A. Paris, Quantum estimation for quantum technology, Int. J. Quantum Inf. **07**, 125 (2009).

[7] S. Pirandola, B. R. Bardhan, T. Gehring, C. Weedbrook, and S. Lloyd, Advances in photonic quantum sensing, Nat. Photonics **12**, 724 (2018).

[8] C. L. Degen, F. Reinhard, and P. Cappellaro, Quantum sensing, Rev. Mod. Phys. **89**, 035002 (2017).

[9] P. C. Humphreys, M. Barbieri, A. Datta, and I. A. Walmsley, Quantum Enhanced Multiple Phase Estimation, Phys. Rev. Lett. **111**, 070403 (2013).

[10] M. D. Vidrighin, G. Donati, M. G. Genoni, X.-M. Jin, W. S. Kolthammer, M. Kim, A. Datta, M. Barbieri, and I. A. Walmsley, Joint estimation of phase and phase diffusion for quantum metrology, Nat. Commun. **5**, 3532 (2014).

[11] M. Gessner, L. Pezzè, and A. Smerzi, Sensitivity Bounds for Multiparameter Quantum Metrology, Phys. Rev. Lett. **121**, 130503 (2018).

[12] R. Demkowicz-Dobrzański, W. Górecki, and M. Guţă, Multi-parameter estimation beyond quantum Fisher information, J. Phys. A: Math. Theor. **53**, 363001 (2020).

[13] J. Liu, H. Yuan, X.-M. Lu, and X. Wang, Quantum Fisher information matrix and multiparameter estimation, J. Phys. A: Math. Theor. **53**, 023001 (2019).

[14] T. J. Proctor, P. A. Knott, and J. A. Dunningham, Multiparameter Estimation in Networked Quantum Sensors, Phys. Rev. Lett. **120**, 080501 (2018).

[15] M. Tsang, H. M. Wiseman, and C. M. Caves, Fundamental Quantum Limit to Waveform Estimation, Phys. Rev. Lett. **106**, 090401 (2011).

[16] C. Lupo and S. Pirandola, Ultimate Precision Bound of Quantum and Subwavelength Imaging, Phys. Rev. Lett. **117**, 190802 (2016).

[17] J. Řehaček, Z. Hradil, B. Stoklasa, M. Paúr, J. Grover, A. Krzic, and L. L. Sánchez-Soto, Multiparameter quantum metrology of incoherent point sources: Towards realistic superresolution, Phys. Rev. A **96**, 062107 (2017).

[18] R. Nichols, P. Liuzzo-Scorpo, P. A. Knott, and G. Adesso, Multiparameter Gaussian quantum metrology, Phys. Rev. A **98**, 012114 (2018).

[19] M. W. Mitchell, J. S. Lundeen, and A. M. Steinberg, Super-resolving phase measurements with a multiphoton entangled state, Nature **429**, 161 (2004).

[20] J. Aasi *et al.*, Enhanced sensitivity of the LIGO gravitational wave detector by using squeezed states of light, Nat. Photonics **7**, 613 (2013).

[21] S. C. Burd, R. Srinivas, J. J. Bollinger, A. C. Wilson, D. J. Wineland, D. Leibfried, D. H. Slichter, and D. T. C. Allcock, Quantum amplification of mechanical oscillator motion, Science **364**, 1163 (2019).

[22] K. C. McCormick, J. Keller, S. C. Burd, D. J. Wineland, A. C. Wilson, and D. Leibfried, Quantum-enhanced sensing of a single-ion mechanical oscillator, Nature **572**, 86 (2019).

[23] F. Wolf, C. Shi, J. C. Heip, M. Gessner, L. Pezzè, A. Smerzi, M. Schulte, K. Hammerer, and P. O. Schmidt, Motional Fock states for quantum-enhanced amplitude and phase measurements with trapped ions, Nat. Commun. **10**, 1 (2019).

[24] T. Baumgratz and A. Datta, Quantum Enhanced Estimation of a Multidimensional Field, Phys. Rev. Lett. **116**, 030801 (2016).

[25] F. Martin Ciurana, G. Colangelo, L. Slodička, R. J. Sewell, and M. W. Mitchell, Entanglement-Enhanced Radio-Frequency Field Detection and Waveform Sensing, Phys. Rev. Lett. **119**, 043603 (2017).

[26] C. Troullinou, R. Jiménez-Martínez, J. Kong, V. G. Lucivero, and M. W. Mitchell, Squeezed-Light Enhancement and Backaction Evasion in a High Sensitivity Optically Pumped Magnetometer, Phys. Rev. Lett. **127**, 193601 (2021).

[27] S. Qvarfort, A. Serafini, P. F. Barker, and S. Bose, Gravimetry through non-linear optomechanics, Nat. Commun. **9**, 1 (2018).

[28] L. Kleybolte, P. Gewecke, A. Sawadsky, M. Korobko, and R. Schnabel, Squeezed-Light Interferometry on a Cryogenically Cooled Micromechanical Membrane, Phys. Rev. Lett. **125**, 213601 (2020).
[29] F. Fogliano, B. Besga, A. Reigue, L. M. de Lépinay, P. Heringlake, C. Gouriou, E. Eyraud, W. Wernsdorfer, B. Pigeau, and O. Arcizet, Ultrasensitive nano-optomechanical force sensor operated at dilution temperatures, Nat. Commun. **12**, 4124 (2021).
[30] H. Nagaoka, in *Asymptotic Theory of Quantum Statistical Inference* (World Scientific, 2005), p. 100.
[31] L. O. Conlon, J. Suzuki, P. K. Lam, and S. M. Assad, Efficient computation of the Nagaoka-Hayashi bound for multiparameter estimation with separable measurements, npj Quantum Inf. **7**, 110 (2021).
[32] R. D. Gill and M. I. Guţă, in *Institute of Mathematical Statistics Collections* (Institute of Mathematical Statistics, 2013), p. 105.
[33] M. G. Genoni, M. G. A. Paris, G. Adesso, H. Nha, P. L. Knight, and M. S. Kim, Optimal estimation of joint parameters in phase space, Phys. Rev. A **87**, 012107 (2013).
[34] K. Duivenvoorden, B. M. Terhal, and D. Weigand, Single-mode displacement sensor, Phys. Rev. A **95**, 012305 (2017).
[35] M. Bradshaw, P. K. Lam, and S. M. Assad, Ultimate precision of joint quadrature parameter estimation with a Gaussian probe, Phys. Rev. A **97**, 012106 (2018).
[36] M. Poggio, M. P. Jura, C. L. Degen, M. A. Topinka, H. J. Mamin, D. Goldhaber-Gordon, and D. Rugar, An off-board quantum point contact as a sensitive detector of cantilever motion, Nat. Phys. **4**, 635 (2008).
[37] C. L. Latune, B. M. Escher, R. L. de Matos Filho, and L. Davidovich, Quantum limit for the measurement of a classical force coupled to a noisy quantum-mechanical oscillator, Phys. Rev. A **88**, 042112 (2013).
[38] C. L. Latune, I. Sinayskiy, and F. Petruccione, Quantum force estimation in arbitrary non-Markovian Gaussian baths, Phys. Rev. A **94**, 052115 (2016).
[39] S. M. Assad, J. Li, Y. Liu, N. Zhao, W. Zhao, P. K. Lam, Z. Y. Ou, and X. Li, Accessible precisions for estimating two conjugate parameters using Gaussian probes, Phys. Rev. Res. **2**, 023182 (2020).
[40] Q. Zhuang, Z. Zhang, and J. H. Shapiro, Distributed quantum sensing using continuous-variable multipartite entanglement, Phys. Rev. A **97**, 032329 (2018).
[41] K. A. Gilmore, M. Affolter, R. J. Lewis-Swan, D. Barberena, E. Jordan, A. M. Rey, and J. J. Bollinger, Quantum-enhanced sensing of displacements and electric fields with two-dimensional trapped-ion crystals, Science **373**, 673 (2021).
[42] M. Mehboudi, M. Moreno-Cardoner, G. D. Chiara, and A. Sanpera, Thermometry precision in strongly correlated ultracold lattice gases, New J. Phys. **17**, 055020 (2015).
[43] C. Oh, K. Park, R. Filip, H. Jeong, and P. Marek, Optical estimation of unitary Gaussian processes without phase reference using Fock states, New J. Phys. **22**, 123039 (2020).
[44] S. Rahimi-Keshari, A. Scherer, A. Mann, A. T. Rezakhani, A. I. Lvovsky, and B. C. Sanders, Quantum process tomography with coherent states, New J. Phys. **13**, 013006 (2011).
[45] D. Šafránek and I. Fuentes, Optimal probe states for the estimation of Gaussian unitary channels, Phys. Rev. A **94**, 062313 (2016).
[46] Y. S. Teo, K. Park, S. Shin, H. Jeong, and P. Marek, Highly accurate Gaussian process tomography with geometrical sets of coherent states, New J. Phys. **23**, 063024 (2021).
[47] F. Albarelli, J. F. Friel, and A. Datta, Evaluating the Holevo Cramér-Rao Bound for Multiparameter Quantum Metrology, Phys. Rev. Lett. **123**, 200503 (2019).
[48] X. Li, Q. Pan, J. Jing, J. Zhang, C. Xie, and K. Peng, Quantum Dense Coding Exploiting a Bright Einstein-Podolsky-Rosen Beam, Phys. Rev. Lett. **88**, 047904 (2002).
[49] N. Takanashi, W. Inokuchi, T. Serikawa, and A. Furusawa, Generation and measurement of a squeezed vacuum up to 100 mHz at 1550 nm with a semi-monolithic optical parametric oscillator designed towards direct coupling with waveguide modules, Opt. Express **27**, 18900 (2019).
[50] T. Kashiwazaki, N. Takanashi, T. Yamashima, T. Kazama, K. Enbutsu, R. Kasahara, T. Umeki, and A. Furusawa, Continuous-wave 6-dB-squeezed light with 2.5-THz-bandwidth from single-mode PPLN waveguide, APL Photonics **5**, 036104 (2020).
[51] E. E. Wollman, C. U. Lei, A. J. Weinstein, J. Suh, A. Kronwald, F. Marquardt, A. A. Clerk, and K. C. Schwab, Quantum squeezing of motion in a mechanical resonator, Science **349**, 952 (2015).
[52] J.-M. Pirkkalainen, E. Damskägg, M. Brandt, F. Massel, and M. A. Sillanpää, Squeezing of Quantum Noise of Motion in a Micromechanical Resonator, Phys. Rev. Lett. **115**, 243601 (2015).
[53] V. Guarrera, R. Gartman, G. Bevilacqua, G. Barontini, and W. Chalupczak, Parametric Amplification and Noise Squeezing in Room Temperature Atomic Vapors, Phys. Rev. Lett. **123**, 033601 (2019).
[54] M. Yukawa, K. Miyata, T. Mizuta, H. Yonezawa, P. Marek, R. Filip, and A. Furusawa, Generating superposition of up-to three photons for continuous variable quantum information processing, Opt. Express **21**, 5529 (2013).
[55] G. Harder, C. Silberhorn, J. Rehacek, Z. Hradil, L. Motka, B. Stoklasa, and L. L. Sánchez-Soto, Local Sampling of the Wigner Function at Telecom Wavelength with Loss-Tolerant Detection of Photon Statistics, Phys. Rev. Lett. **116**, 133601 (2016).
[56] M. Cooper, L. J. Wright, C. Söller, and B. J. Smith, Experimental generation of multi-photon Fock states, Opt. Express **21**, 5309 (2013).
[57] M. Bohmann, J. Tiedau, T. Bartley, J. Sperling, C. Silberhorn, and W. Vogel, Incomplete Detection of Nonclassical Phase-Space Distributions, Phys. Rev. Lett. **120**, 063607 (2018).
[58] E. Chitambar and G. Gour, Quantum resource theories, Rev. Mod. Phys. **91**, 025001 (2019).